


## A novel dendrimer-based complex co-modified with cyclic RGD hexapeptide and penetratin for noninvasive targeting and penetration of the ocular posterior segment

Xiucheng Yang<sup>a</sup> , Lihua Wang<sup>b</sup>, Lin Li<sup>a</sup>, Meishan Han<sup>a</sup>, Shengnan Tang<sup>a</sup>, Tengteng Wang<sup>a</sup>, Junping Han<sup>a</sup>, Xiaoyan He<sup>a</sup>, Xiuting He<sup>a</sup>, Aiping Wang<sup>a,c</sup> and Kaoxiang Sun<sup>a</sup>

<sup>a</sup>School of Pharmacy, Collaborative Innovation Center of Advanced Drug Delivery System and Biotech Drugs in Universities of Shandong, Key Laboratory of Molecular Pharmacology and Drug Evaluation (Yantai University), Ministry of Education, Yantai University, Yantai, China; <sup>b</sup>School Hospital of Yantai University, Yantai, China; <sup>c</sup>State Key Laboratory of Long-Acting and Targeting Drug Delivery System, Shandong Luye Pharmaceutical Co. Ltd., Yantai, China

### ABSTRACT

Noninvasive drug delivery is a promising treatment strategy for ocular posterior segment diseases. Many physiological and anatomical barriers of the eye considerably restrict effective diffusion of therapeutics to the target site. To overcome this problem, a novel cyclic arginine-glycine-aspartate (RGD) hexapeptide and penetratin (PEN) co-modified PEGylation polyamidoamine (PAMAM) was designed as a nanocarriers (NCs), and its penetrating and targeting abilities were evaluated. In this study, we show that PAMAM-PEG (reaction molar ratio 1:32) has a relatively high grafting efficiency and low cytotoxicity. The particle size was within the range of 15–20 nm after modification with RGD and PEN. Cellular uptake of RGD-modified NCs involved significant affinity toward integrin  $\alpha v \beta 3$ , which validated the targeting of neovasculature. An *in vitro* permeation study indicated that modification with PEN significantly improved penetration of the NCs (1.5 times higher). *In vivo* ocular distribution studies showed that, the NCs (modified with PEN or co-modified with RGD and PEN) were highly distributed in the cornea and retina ( $p < .001$ ), and modification extended retinal retention time for more than 12 h. Therefore, these NCs appear to be a promising noninvasive ocular drug delivery system for ocular posterior segment diseases.

### ARTICLE HISTORY

Received 16 August 2019  
Revised 30 August 2019  
Accepted 10 September 2019

### KEYWORDS

PAMAM dendrimer; cyclic RGD hexapeptide; penetratin; nanocarriers; ocular posterior segment

### Introduction

Age-related macular degeneration (AMD) causes gradual blindness and is temporarily incurable (Pennington & DeAngelis, 2016). In the United States alone, approximately 11 million people are affected by AMD, global prevalence has reached 170 million, and the number of people projected to have AMD in 2040 is 288 million (Wong et al., 2014). As the population ages, the incidence rate will increase. AMD can be divided into exudative AMD and non-exudative AMD. Although the exudative AMD associated with only 15% of AMD cases, it is responsible for a significant proportion of cases of vision loss associated with AMD (Votruba & Gregor, 2001). Previous studies have shown that choroidal neovascularization (CNV) plays a key role in acute visual loss in AMD (Ambati et al., 2003).

At present, intravitreal injection of anti-angiogenic antibodies is the first choice for exudative AMD therapy (Heier et al., 2012). According to a long-term study (Rofagha et al., 2013), such therapies have improved the prospects of patients with exudative AMD. However, the risk of vision-threatening complex diseases such as lens injury, vitreous hemorrhage, retinal detachment and endophthalmitis is increased by invasive interventions (Thakur et al., 2014). In

addition, subconjunctival injection may be an alternative, but it is still invasive. Fortunately, eye drops, which are an alternative to eye injections for the treatment of posterior segment diseases, are in development (Li et al., 2019). However, because the many physiological and anatomical barriers in the eye considerably restrict effective diffusion of therapeutics to the target site (Peynshaert et al., 2018), the penetration and targeting of eye drops still needs to be improved.

Dendrimers are spherical dendritic nanometer-sized (3–20 nm) polymers (Xu et al., 2013). Drugs can be embedded in polymer networks through ionic interactions, hydrophobic interactions and hydrogen bonds. In addition, they can be also coupled using chemical bonds (Madaan et al., 2016). In dendrimers, polyamidoamine (PAMAM) is one of the most studied and commercially exploited species for therapeutic agent delivery. PAMAM dendrimers are water-soluble and non-immunogenic, and the biocompatibility of PAMAM can be increased through modification with poly(ethylene glycol) (PEG) (Malik et al., 2000; Jevprasesphant et al., 2003). Our previous studies have shown that PAMAM can increase the corneal permeability and improve the bio-availability of a co-delivered drug (Yao et al., 2011). Therefore, in the current study, we constructed a PAMAM-

based nanometer-sized ocular drug delivery system through surface structural modification.

The RGD peptide sequence can bind integrin  $\alpha v \beta 3$ . Integrin  $\alpha v \beta 3$  is pivotal for neovascularization, and is upregulated during this process (Millard et al., 2011). During CNV pathogenesis, integrin expression dramatically increases, and conversely, integrin expression is minimal in the healthy choroid (Hennig & Goepferich, 2015). In our previous studies, we found that the cyclic hexapeptide of c(RGDf(N-me)VK) exhibited strong affinity for integrin  $\alpha v \beta 3$ -overexpressing cells (Zhang et al., 2017). Furthermore, the cyclic peptides showed a potent inhibitory effect on CNV, because of their ability to antagonize integrins after binding (Luo et al., 2013). Therefore, we selected this new cyclic hexapeptide as a targeting ligand, and applied it to ocular drug delivery for the first time.

Although the eye is an easily accessible organ, various ocular barriers such as the sclera, conjunctiva, and cornea, lead to difficulties in drug delivery to the ocular posterior segment (Nayak & Misra, 2018). In addition, the viscoelastic mucus of the ocular surface can trap and quickly eliminate nanoparticle-based drug delivery systems, therefore restricting targeted and sustained drug delivery at the ocular surface. A series of studies has shown that a relatively dense grafting of medium molecular weight PEG (e.g. 2–5 kDa) results in a dense brush conformation, which can efficiently avoid contact with mucins and promote rapid penetration of nanoparticles in mucus (Xu et al., 2015; Huckaby & Lai, 2018). In positively charged cell penetrating peptides (CPPs) usually composed of less than 30 amino acids, the amino acid sequences have a wide range of sources, and can transport macromolecules into living cells and cross many physiological barriers (Patel et al., 2007). Unlike intravenous injection and oral administration, CPP-mediated drug delivery for ocular application has not yet been researched widely. Research has shown that among the studied CPPs, penetratin (RQIKIWFQNRRMKWKKK) shows excellent performance in terms of high permeability of the posterior segment, and high biocompatibility (Liu et al., 2014).

To maximize both targeting of the CNV and crossing of the ocular physiological barriers, in the current study, RGD and PEN co-modified PEGylated PAMAM was successfully constructed. It was possible to adjust the size by changing the molecular weight and grafting density of the PEG. Fluorescein isothiocyanate (FITC) was used as a fluorescent probe for cell and animal imaging experiments and it was linked to PAMAM. The cytotoxicity of NCs in human conjunctival epithelial cells (NHCs), human corneal epithelial cells (HCECs), and human umbilical vein endothelial cells (HUVECs) was measured using a MTT assay. Because of the wide application of HUVECs as vascular endothelial cells in investigations of pathologic neovascularization, HUVECs were applied as a cellular model to validate the targeting of the NCs. The in vitro permeability of the NCs was evaluated in NHCs and HCECs. Furthermore, frozen sections of mouse eyes were used to evaluate the in vivo distribution of NCs. The penetration and targeting of the NCs were studied to identify their availability and feasibility for use in the treatment of ocular posterior segment diseases. We hope that the

current research will contribute to the development of a noninvasive CNV eyedrop treatment.

## Materials and methods

### Materials and animals

PAMAM G4.0 was obtained from Sigma-Aldrich, Inc. (St. Louis, MO). Methoxy PEG succinimidyl carboxymethyl ester (M-PEG-SCM, MW = 2000 Da) and Maleimide PEG succinimidyl carboxymethyl ester (MAL-PEG-SCM, MW = 2000 Da) were provided by JenKem Technology Co., Ltd. (Beijing, China). c(RGDf(N-me)VK)-C (MW = 820 Da) was obtained from Shanghai Top-Peptide Biotechnology Co., Ltd. (Shanghai, China). Penetratin (C-RQIKIWFQNRRMKWKK, MW = 2350 Da) was obtained from ChinaPeptides Co., Ltd. (Shanghai, China). Artificial tear fluid was composed of 0.65 mM  $\text{CaCl}_2 \cdot \text{H}_2\text{O}$ , 18.51 mM KCl, 25.95 mM  $\text{NaHCO}_3$ , and 116.02 mM NaCl in deionized water.

Dulbecco's modified eagle medium (DMEM)/high glucose and trypsin solution were obtained from HyClone (Logan, UT, USA). Penicillin-streptomycin solution, 3-(4,5-dimethylthiazol-2-yl)-2,5-diphenyltetrazolium bromide (MTT), and phosphate-buffered saline (PBS, pH 7.4) were obtained from Beyotime Biotechnology Co., Ltd. (Shanghai, China). Bis benzimide Hoechst NO33342, rat tail tendon collagen type, hank's balanced salt solution (HBSS) and O.C.T. compound were obtained from Beijing Solarbio Science & Technology Co., Ltd. (Beijing, China). Fetal bovine serum (FBS) was bought from Zhejiang Tianhang Biological Technology Co., Ltd. (Zhejiang, China). Davidson's solution was composed of 50 mL acetic acid, 150 mL 95% ethanol, 100 mL 10% neutral buffer formaldehyde solution and 150 mL distilled water.

NHCs, HCECs, and HUVECs were provided by Cellbio Bioengineering Co., Ltd. (Shanghai, China). Male ICR mice (40 g  $\pm$  5 g) were obtained from Jinan Pengyue Laboratory Animal Breeding Co., Ltd. (Shandong, China). Animal experiments were carried out in accordance with the UK Animals (Scientific Procedures) Act, 1986, and associated guidelines, and the EU Directive 2010/63/EU for animal experiments.

### Synthesis and characterization of NCs

RGD and PEN were connected to the primary amine groups of PAMAM via MAL-PEG-SCM. For the purpose of tracing the cellular uptake, in vitro permeability, and in vivo ocular distribution of the synthetic carriers, FITC was used as a fluorescent probe and we synthesized the following NCs: FITC-PAMAM (FP), FITC-PAMAM-PEG $_n$  ( $n = 8, 16, 32,$  and 48), FITC-PAMAM-PEG32-RGD (FPPR), FITC-PAMAM-PEG32-PEN (FPPP), and FITC-PAMAM-PEG32-RGD/PEN (FPPRP) conjugates. The synthetic routes are shown in Figure 1.

### Synthesis of FP conjugates

FITC (2.72 mg, 7.0  $\mu\text{mol}$ ) dissolved in 3 mL of methanol was added to 3 mL of a PAMAM (20 mg, 1.4  $\mu\text{mol}$ ) methanol solution. The reaction system was stirred for 12 h in dark

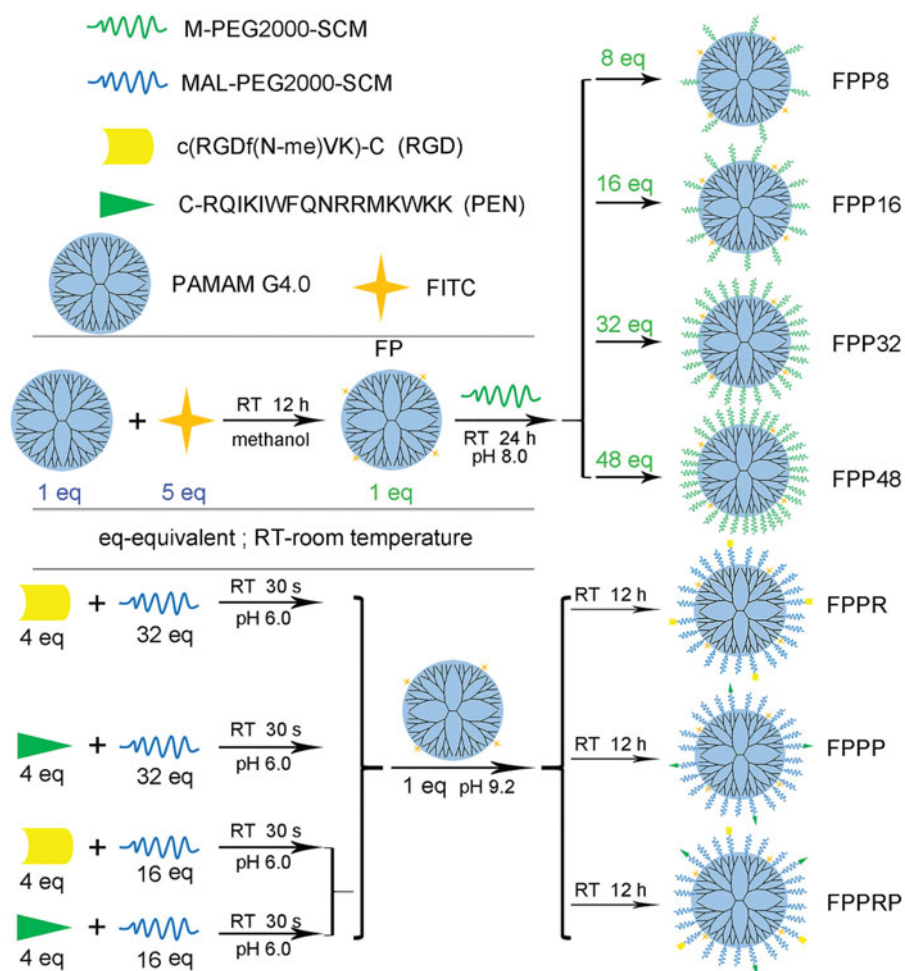


**Figure 1.** Synthetic routes of FP, FPP, FPPR, FPPP, and FPPRP.

conditions at room temperature (RT). The reaction product was purified through dialysis against water using a dialysis membrane (MWCO = 3500 Da) for 24 h in darkness. The obtained solution was concentrated using an ultrafiltration tube (MWCO = 3000 Da) until the filtrate was colorless and it was lyophilized to obtain FP.

### Synthesis of FPPn conjugates

FPPn was constructed through the reaction of the primary amine groups of the FP with the SCM groups of M-PEG-SCM. FPPn was constructed with various degrees of PEGylation. Different quantities of PEG (9.9 mg, 4.95  $\mu\text{mol}$ ; 19.8 mg, 9.91  $\mu\text{mol}$ ; 39.6 mg, 19.8  $\mu\text{mol}$ ; 59.5 mg, 29.7  $\mu\text{mol}$ ) were added to 6 mL of PBS (0.2 M, pH 8.0) containing FP (10 mg, 0.62  $\mu\text{mol}$ ). The reaction systems were stirred for 24 h at RT, with nitrogen blanketing and away from light. The mixtures were purified via dialysis against water using a dialysis membrane (MWCO = 7000 Da) for 24 h in darkness. The obtained solution was concentrated using an ultrafiltration tube (MWCO = 10000 Da) until the PEG was eliminated from the filtrate, which was verified through thin layer chromatography (TLC). The reaction products were lyophilized to acquire FPP8, FPP16, FPP32, and FPP48.

### Synthesis of FPPR, FPPP, and FPPRP conjugates

RGD peptides were linked to FP to synthesize FPPR through MAL-PEG-SCM. PEG (39.7 mg, 19.8  $\mu\text{mol}$ ) and RGD (2.0 mg, 2.5  $\mu\text{mol}$ ) were dissolved in 3 mL of NaAc-HAc buffer (0.1 M, pH 6.0) and reacted for 30 s, and then transferred to 3 mL of NaOH-borax buffer (0.05 M, pH 9.2) with FP (10 mg, 0.62  $\mu\text{mol}$ ) and stirred for 12 h in the dark at RT, with nitrogen blanketing. Considering that the unreacted maleimide may affect the in vivo behavior of the NCs, the pH of the reaction system was adjusted to 7, and an excess of 2-mercaptoethanol was added to the reaction for 1 h (Zhu et al., 2011). The product was purified via dialysis against water using a dialysis membrane (MWCO = 7000 Da) for 24 h in darkness. The obtained solution was concentrated using an ultrafiltration tube (MWCO = 30000 Da) until the PEG and RGD were eliminated from the filtrate, which was verified through TLC. After vacuum freeze drying, FPPR was obtained. Similarly, PEN peptides (5.8 mg, 2.5  $\mu\text{mol}$ ) were linked to FP (10 mg, 0.62  $\mu\text{mol}$ ) to synthesize FPPP via PEG (39.7 mg, 19.8  $\mu\text{mol}$ ).

Furthermore, FPPRP was also constructed using the above method. Briefly, RGD (2.0 mg, 2.5  $\mu\text{mol}$ ) plus PEG (19.8 mg, 9.9  $\mu\text{mol}$ ) and PEN (5.8 mg, 2.5  $\mu\text{mol}$ ) plus PEG (19.8 mg, 9.9  $\mu\text{mol}$ ), were dissolved in 1.5 mL of NaAc-HAc buffer (0.1 M, pH 6.0), respectively. After stirring for 30 s, they were added in turn to 3 mL of NaOH-borax buffer (0.05 M, pH 9.2)

with FP (10 mg, 0.62  $\mu\text{mol}$ ). After the reaction, purification, and lyophilization steps, FPPRP was acquired.

### Characterization of synthetic NCs

The structure of the modified PAMAM samples was confirmed through nuclear magnetic resonance using a proton nuclear magnetic resonance ( $^1\text{H}$  NMR) spectrometer (400 MHz; JEOL, Tokyo, Japan). The average diameter, zeta potential, and size distribution of the NCs was measured using a dynamic light scattering (DLS) particle size analyzer (Zetasizer Nano ZSE; Malvern Panalytical, Malvern, UK). The morphology and size of the NCs was examined using a transmission electron microscope (TEM) (JEM-1400Flash; Hitachi, Tokyo, Japan).

### In vitro cell studies

#### In vitro cytotoxicity assay

NHCs, HCECs, and HUVECs were cultured at 37 °C in a humid atmosphere at 5%  $\text{CO}_2$  wet air in DMEM/high glucose plus 10% FBS, 100 mg/mL streptomycin sulfate antibiotics, and 100 IU/mL penicillin.

The cytotoxicity of NCs in NHCs, HCECs, and HUVECs was evaluated using an MTT assay. Briefly, when the cells entered the logarithmic growth phase, they were digested and inoculated in 96-well plates (3000 cells/well) and incubated for 24 h. The original culture solution was removed and 100  $\mu\text{L}$  of fresh culture medium with different concentrations (0.2, 0.5, 1, 2, 5, 10, and 20  $\mu\text{M}$ ) of NCs was added, and then the cells were cultured for 6 or 24 h. After that, 20  $\mu\text{L}$  of MTT aqueous solution was added and incubated for 4 h. Then, the media was removed, and 150  $\mu\text{L}$  of dimethyl sulfoxide was added. Finally, the absorbance was measured using a CYTATION 5 imaging reader (BioTek Instruments, Winooski, VT, USA) at a wavelength of 570 nm after gentle shaking for 10 min. Negative control groups without NCs were established at the same time.

#### Cellular uptake study

The cellular uptake of NCs was visualized using an inverted fluorescence microscope (Vert.A1; Carl Zeiss AG, Oberkochen, Germany). NHCs, HCECs, and HUVECs were inoculated into 24-well plates (30,000 cells/well) and cultivated for 24 h, and then NCs (2  $\mu\text{M}$ ) were added and cultivated for 6 h. After 0.5, 1, 2, 4, and 6 h of cultivation, the cells were rinsed three times using and fixed using polyformaldehyde (4%). Finally, the cells were observed after negative staining of nuclei using Hoechst 33342 (5  $\mu\text{g}/\text{mL}$ ).

Flow cytometry was used to quantify the cellular uptake of NCs. Briefly, NHCs, HCECs, and HUVECs were inoculated into 6-well plates (3,00,000 cells/well) and cultivated for 24 h, and then NCs (2  $\mu\text{M}$ ) were added and cultivated for 4 h. After 0.5, 1, 2, and 4 h of cultivation, the cells were digested and centrifuged (1500 rpm for 5 min) and washed with PBS three times. Finally, flow cytometry was used to detect the average FITC fluorescence intensity of the cells.

### In vitro corneal and conjunctival permeation

NHCs and HCECs were inoculated in transwell plates at 50,000 cells/well and cultivated for 3–4 weeks until the trans-epithelial electrical resistance (TEER) was 200–300  $\Omega/\text{cm}^2$  (Toropainen et al., 2001). Specifically, 0.5 mL of medium containing the cells was added to each 12 mm Transwell with a 0.4  $\mu\text{m}$  pore polycarbonate membrane insert (coated with rat tail tendon collagen type I), and 1.5 mL of blank medium was added to the basolateral side. The color of the medium was observed every day, and when it changed from pink to light yellow, the medium was replaced. From the third week, the TEER value was monitored using a Millicell ERS meter (Millipore Corporation, Bedford, MA, USA). When the TEER value of the cell layers was greater than 200  $\Omega/\text{cm}^2$ , they were used for in vitro transport studies.

When the TEER value of each chamber reached the experimental requirement, the medium in the well plate was removed, and the cell layer was washed using preheated HBSS. Next, 1.5 mL of HBSS was added to the lower chamber, and then 0.5 mL of medium containing FPP, FPPR, FPPP and FPPRP was added to the upper chambers at a concentration of 5  $\mu\text{M}$  and the samples were cultivated for 4 h at 37 °C. At 0.5, 1, 2, 3, and 4 h, 0.2 mL of sample was removed from the lower chamber and an equal amount of HBSS was added. Finally, a standard curve was established using a microplate reader at a wavelength of 488 nm, and the amount of NCs in each sample was calculated. The following formula was used to calculate the apparent permeability of the NCs:

$$P_{\text{app}} = \frac{\Delta Q}{\Delta t} \times \frac{1}{AC_0}$$

where  $P_{\text{app}}$  is the apparent permeability (cm/s), the total amount of NCs transported to the lower chamber is represented by  $\Delta Q$  ( $\mu\text{g}$ ),  $A$  is the area of the upper chamber (1.12  $\text{cm}^2$ ), and the original concentration of NCs in the upper chamber is represented by  $C_0$  ( $\mu\text{g}/\text{mL}$ ).

### In vivo ocular distribution

The intraocular distribution of NCs was studied after topical instillation. Briefly, we dissolved NCs in artificial tear fluid (20  $\mu\text{M}$ ), and then instilled 5  $\mu\text{L}$  into the conjunctival sac of mice three times in 30 min (Liu et al., 2016). The eyelids were pulled up and closed lightly to spread the NCs on the ocular surface. After the last administration, the mice were sacrificed at 1, 2, 4, 8, 12, and 24, and then the eyeballs were excised and rinsed with artificial tear fluid. The excised eyeballs were fixed in Davidson's solution for 30 min and then embedded in OCT compound. Corneal and retinal images of frozen sections (15  $\mu\text{m}$  thick) were obtained using an inverted fluorescence microscope with fluorescence filters for FITC. The fluorescence intensity of FITC was evaluated using ImageJ software (Suda et al., 2017).

### Data analysis

The data are shown as the means  $\pm$  standard deviations (SD). Statistical comparisons were evaluated using two-sample  $t$



tests and one-way analysis of variance. A  $p$  value of .05 or less was considered statistically significant.

## Results and discussion

### Characterization of synthetic NCs

The successful construction of FP, FPP, FPPR, FPPP, and FPPRP was confirmed through  $^1\text{H}$  NMR. The characteristic peaks of PAMAM, RGD, and PEN are shown in Figure 2(A,D,F), and a detailed assignment of the characteristic peaks was carried out. Briefly, the presence of the aromatic proton peaks demonstrated the successful synthesis of FP (Figure 2(B)). The successful synthesis of FPP was demonstrated by the disappearance of the succinimidyl proton peaks and the appearance of an obvious signal at 3.7 ppm that accorded with the methylene proton of PEG. The presence of the isopropyl group proton peaks (Figure 2(E-d)) at 0.6 and 0.9 ppm demonstrated the successful synthesis of FPPR, and the presence of the mercaptomethyl proton peaks (Figure 2(G-d)) at 1.9 ppm demonstrated the successful synthesis of FPPP. Finally, as mentioned earlier, the successful construction of FPPRP was identified by the occurrence of a signal at approximately 0.55 ppm that corresponded to the isopropyl group protons (Figure 2(D-a)) of RGD, and a signal at approximately 1.9 ppm that corresponded to the mercaptomethyl protons (Figure 2(F-d)) of PEN. In addition, the number of FITC, PEG, and polypeptide molecules coupled per molecule of PAMAM was calculated using peak area normalization method, which involves the relative integration values of the peaks (Luo et al., 2002).

The number of FITC, PEG, and polypeptide molecules coupled per molecule of PAMAM and the grafting efficiency are shown in Table 1. As the feed molar ratio increased, the conjugated number of PEG molecules per PAMAM molecule also increased, but the grafting efficiency decreased, indicating that the previously reacted PEG molecules produced steric hindrance for subsequent reaction, thereby affecting the grafting efficiency. The phenomenon became very obvious when the feed molar ratio was increased to 48:1. Particle size can significantly affect the drug delivery efficiency of nanoparticles, and the smaller the particle size, the larger the specific surface area, resulting in a larger contact area with the ocular surface (Yoncheva et al., 2005). In brief, small nanoparticles appear to have significant size advantages when used for ocular drug delivery. Fortunately, this small size is a crucial feature of modified PAMAM, and previous research (Inokuchi et al., 2010) has shown that when drugs are delivered to the ocular posterior segment through topical administration, smaller nanoparticles tend to have higher delivery efficiency. In addition, a previous study suggested that particles which are too small (<5 nm), such as gold nanoparticles, are rapidly eliminated from the target tissues (Jain & Stylianopoulos, 2010). In addition, the biocompatibility of PAMAM can be improved through PEG modification, and this is dependent on the degree of PEGylation (Li et al., 2016). Based on these phenomena, we chose FPP32 for further research.

In aqueous solution, PAMAM G4.0 existed as nanoparticles with a particle size of 5.63 nm (Thanh et al., 2018), and the size significantly increased after modification (Table 1). The morphology and size distribution of the NCs were determined using DLS and TEM, and the results are presented in Figure 3. As the degree of PEGylation increases, the particle size becomes larger, and we found that the particles demonstrated a broader size range than that of FPP after polypeptide modification. In addition, the number of surface primary amine groups decreased with PEG modification, leading to a reduction in zeta potential. Modification with RGD and PEN led to a small increase in zeta potential, which is mainly caused by the lysine (K) and arginine (R) in the polypeptides.

### In vitro cell study

#### In vitro cytotoxicity

To evaluate the safety of NCs for ocular administration and determine the concentration for subsequent cell experiments, the cellular viability of NHCs, HCECs, and HUVECs was evaluated through MTT assays. Considering the residence time of NCs on the surface of the eye and the timing of subsequent cell experiments, the duration of the cytotoxicity experiment was set at 6 h. As shown in Figure 4(A–C), the percentage cell survival was 90%–110% after incubation with 0.2–20  $\mu\text{M}$  NCs, confirming that NCs are not significantly cytotoxic.

Some studies have shown that generation number and surface functional groups can significantly affect the cytotoxicity of dendrimers, and surface functional groups play a pivotal role in controlling cytotoxic properties (Mignani et al., 2018). Simple modifications of the surface functional groups, such as the addition of carbohydrate units and peptides, grafting amino acids, and acetylation and PEGylation, can increase biocompatibility (Mishra et al., 2009). For the purpose of studying the role of PEGylation and polypeptide modification the current study, the NCs were cultivated with cells for 24 h. Survival curves were constructed following MTT assays (Figure 4(D–F)) and these demonstrate that the cytotoxicity of PAMAM can be significantly decreased through PEG modification ( $p < .01$  at 20  $\mu\text{M}$ , FP versus other NCs). Some studies have shown that hemolysis toxicity and cytotoxicity resulted from the abundant surface amino groups of PAMAM (Jevprasesphant et al., 2003), while the PEGylated PAMAM demonstrated lower toxicity because of reduced surface amino groups. In addition, the probability of contact between cells and primary amines was reduced because of the long chains of PEG on the surface of the PAMAM. The survival curves illustrate that PEGylated NCs did not produce obvious cytotoxicity at a concentration lower than 10  $\mu\text{M}$  (cell viability >80%). Moreover, the NHCs and HCECs appear to tolerate PEGylated NCs better than the HUVECs because the survival rate of HUVECs exposed to 20  $\mu\text{M}$  NCs was significantly lower ( $p < .01$ , NHCs and HCECs versus HUVECs). In HUVECs, the cytotoxicity of the NCs had a significant concentration dependence (Figure 4(F)). In addition, compared with HCECs, the other two cell types appeared to be more sensitive to FPPR ( $p < .01$  at 20  $\mu\text{M}$ , NHCs and HUVECs versus

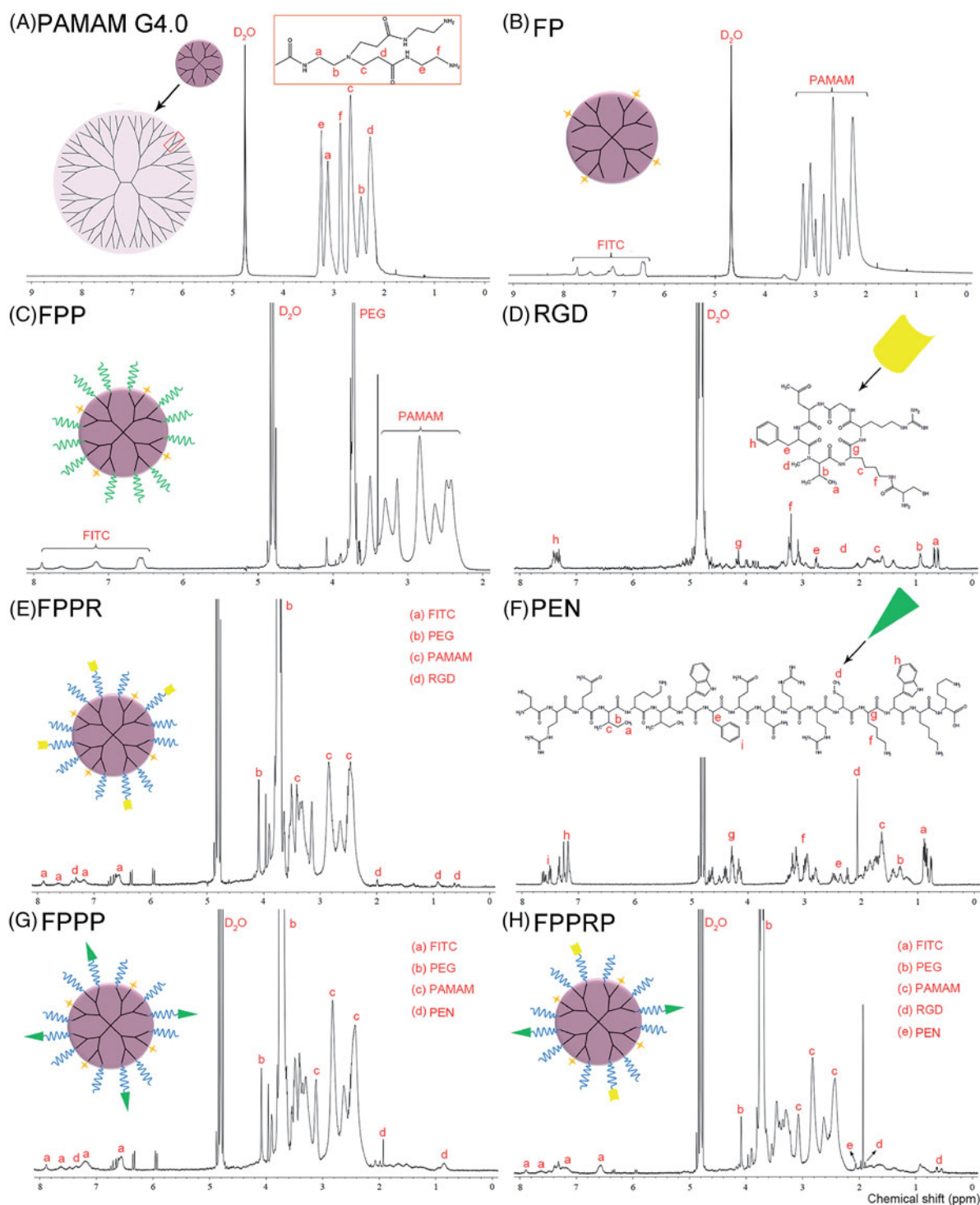


**Figure 2.**  $^1\text{H}$  NMR spectra of PAMAM G4.0 (A), FP (B), FPP (C), RGD (D), FPPR (E), PEN (F), FPPP (G), and FPPRP (H) in  $\text{D}_2\text{O}$ .

HCECs). Compared with FPP, FPPP, and FPPRP, higher cytotoxicity was observed with FPPR (Figure 4(D,F)), probably because the RGD lead to apoptosis (Huang et al., 2007). In our opinion, this may be related to the strong affinity that RGD has for integrin  $\alpha\text{v}\beta3$ -overexpressing cells, such as HUVECs, because of their ability to antagonize integrins after binding. The cornea is mainly composed of avascular connective tissue, but the conjunctiva is rich in blood vessels, and the integrin  $\alpha\text{v}\beta3$  is pivotal for neovascularization, so we

speculate that HCECs are less sensitive to FPPR because of their low expression of integrin  $\alpha\text{v}\beta3$ .

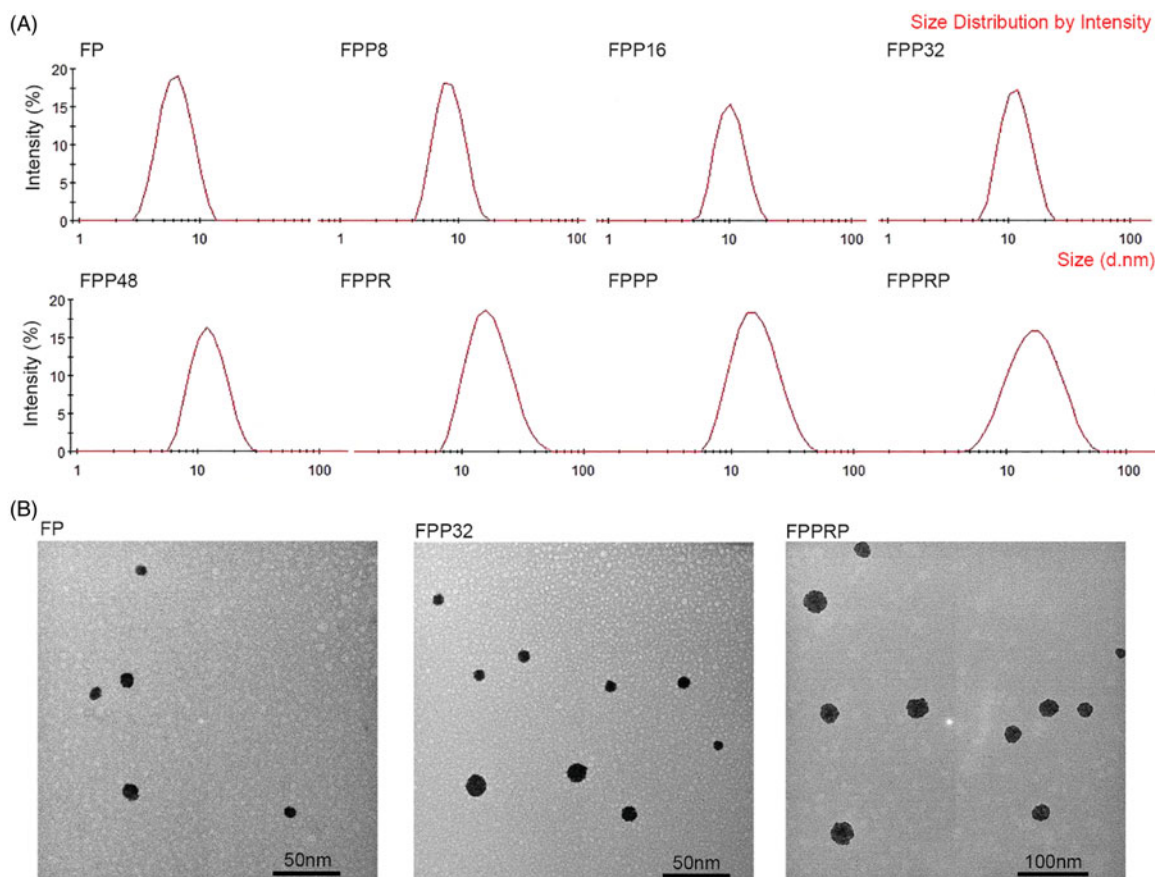
#### Cellular uptake study

The cellular uptake efficiency of FPP, FPPR, FPPP and FPPRP complexes were investigated using fluorescence microscopy for qualitative results and flow cytometry for quantitative results. To evaluate the cell-penetration of PEN-modified NCs

**Table 1.** Characterization of NCs ( $n = 3$ , mean  $\pm$  SD).

| NCs   | Conjugated number per PAMAM (*) |            |           |           | Particle size (nm) | Zeta potential (mV) |
|-------|---------------------------------|------------|-----------|-----------|--------------------|---------------------|
|       | FITC                            | PEG        | RGD       | PEN       |                    |                     |
| FP    | 4.4 (88%)                       | N/A        | N/A       | N/A       | 6.46 $\pm$ 0.14    | 14.22 $\pm$ 0.42    |
| FPP8  | 4.4 (88%)                       | 6.8 (85%)  | N/A       | N/A       | 8.53 $\pm$ 0.19    | 11.7 $\pm$ 0.47     |
| FPP16 | 4.4 (88%)                       | 12.8 (80%) | N/A       | N/A       | 10.39 $\pm$ 0.23   | 9.86 $\pm$ 0.59     |
| FPP32 | 4.4 (88%)                       | 24.2 (76%) | N/A       | N/A       | 11.78 $\pm$ 0.17   | 3.72 $\pm$ 0.55     |
| FPP48 | 4.4 (88%)                       | 30.7 (64%) | N/A       | N/A       | 12.79 $\pm$ 0.35   | 2.93 $\pm$ 0.68     |
| FPPR  | 4.4 (88%)                       | 24.2 (76%) | 3.7 (93%) | N/A       | 16.78 $\pm$ 0.33   | 4.68 $\pm$ 0.49     |
| FPPP  | 4.4 (88%)                       | 24.2 (76%) | N/A       | 3.8 (96%) | 17.75 $\pm$ 0.29   | 6.30 $\pm$ 0.41     |
| FPPRP | 4.4 (88%)                       | 24.2 (76%) | 2.8 (70%) | 3.1 (77%) | 19.16 $\pm$ 0.41   | 6.74 $\pm$ 0.37     |

\*Grafting efficiency of the FITC, PEG, RGD, and PEN modified PAMAMA was calculated from the ratio of the observed connectivity value to the theoretical connectivity value.

**Figure 3.** DLS images (A) and TEM (B) characterizations of NCs.

and the targeting of RGD-modified NCs, we selected NHCs, HCECs, and HUVECs (high expression of integrin  $\alpha v \beta 3$ , the cell model for pathological neovascularization) for cellular uptake research in vitro.

The time-dependent uptake of NCs in NHCs, HCECs, and HUVECs was investigated at 0.5, 1, 2, 4, and 6 h using an inverted fluorescence microscope (Figure 5(A-C)). Fluorescence imaging showed that the blue nuclei are surrounded by green NCs, and the cellular uptake of NCs was enhanced with increasing incubation time, indicating that cellular uptake occurred through active transport. The fluorescence intensity of FPPP and FPPRP was significantly higher than that of FPP and FPPR at different times (Figure 5(A,B)), indicating that PEN modification promoted the uptake of NCs. The fluorescence intensity of the different NCs was

ranked as: FPPP  $\approx$  FPPRP  $>$  FPPR  $>$  FPP, showing that the NCs modified with RGD had increased performance in terms of integrin  $\alpha v \beta 3$  targeting and cellular uptake (Figure 5(C)).

Quantitative measurements of NCs uptake by NHCs, HCECs, and HUVECs were obtained through flow cytometry. The mean fluorescence intensity of the FPPP and FPPRP groups was significantly higher than that of the FPP and FPPR groups at different times ( $p < .001$  or  $p < .01$ , FPPP and FPPRP versus FPP and FPPR; Figure 5(D-F)). This may have been caused by PEN-mediated energy-dependent endocytosis (Zhang et al., 2016). Although extensive research has been conducted into the transmembrane penetration mechanism of CPPs, there is still no clear explanation for this process (Wang et al., 2014), and we believe that cationization and the positive charge of PEN may play a pivotal role in

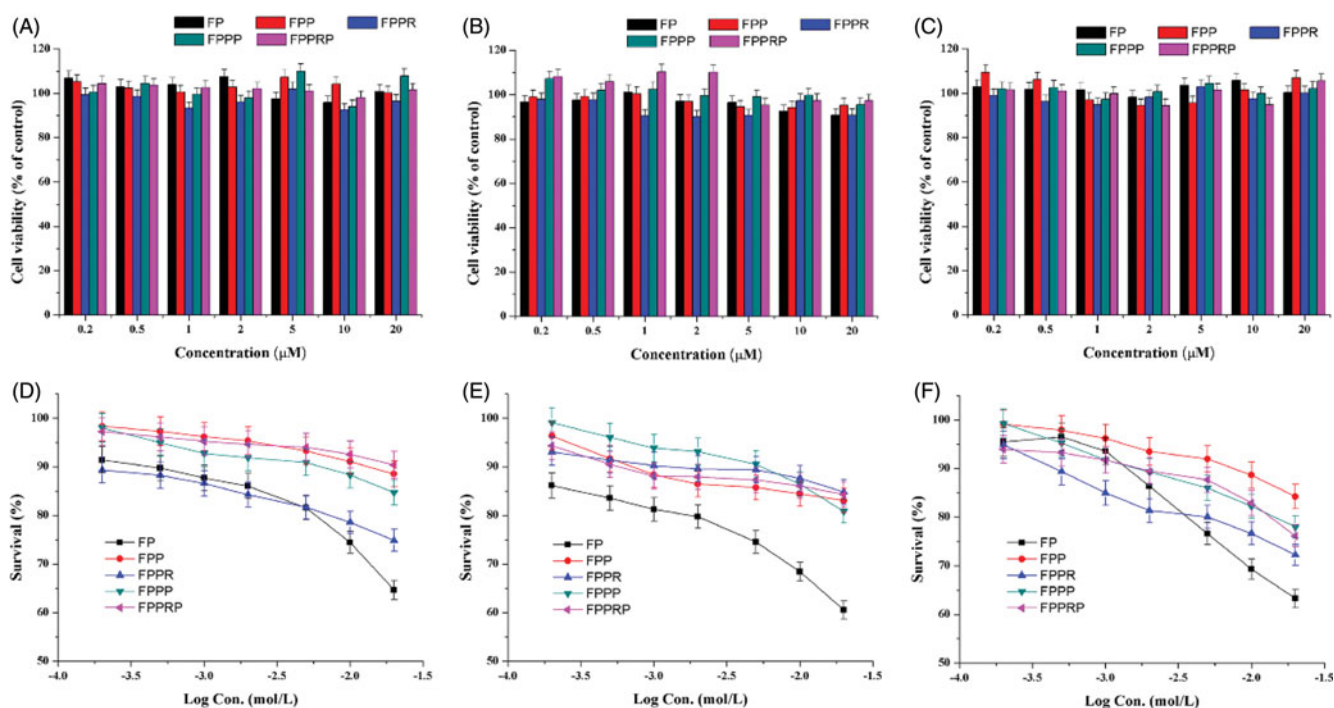


**Figure 4.** In vitro cytotoxicity of the FP, FPP, FPPR, FPPP and FPPRP in NHCs (A), HCECs (B) and HUVECs (C) at concentrations that ranged from 0.2 to 20  $\mu\text{M}$  for 6 h. Cell viability of NHCs (D), HCECs (E), and HUVECs (F) following 24 h incubation with increasing concentrations of various NCs as determined by the MTT assay. ( $n = 5$ , mean  $\pm$  SD).

cellular uptake. In addition, the mean fluorescence intensity of the FPPR group was stronger than that of the FPP group ( $p < .01$  or  $p < .05$ , FPPR versus FPP; Figure 5(D,F)). This indicated that RGD-modified NCs not only had specific recognition abilities for HUVECs but also demonstrated enhanced cellular uptake through ligand-receptor recognition. This also validated the targeting of NCs to neovascularization at the cellular level. Compared with HCECs, we found that the mean fluorescence intensity in NHCs was higher. The cornea and conjunctiva are the first barriers for drugs intended to reach the ocular posterior segment. PEN-mediated NCs appear to reach the ocular posterior segment through both the conjunctival and corneal pathways, but primarily through the conjunctival pathway.

Although they efficiently mediate the cellular uptake of different nanoparticles, CPPs have many problems in the context of in vivo drug delivery, particularly the nonspecific binding and off target delivery. Although intelligent drug delivery systems on the basis of micro environmental characteristics specific to the targeted tissues have been designed (Koren & Torchilin, 2012), this does not apply to the ocular posterior segment, and CPPs must be exposed for penetration of the eye barrier. Therefore, RGD and PEN co-modified NCs were designed to increase targeting efficiency.

### In vitro corneal and conjunctiva permeation

In previous studies, a model of drug and formulation permeability was established using immortalized HCECs (Chu et al., 2017), and the TEER and permeability of the model were similar to those of a complete cornea. Therefore, this in vitro cell model may be used to study the corneal permeability of

drugs and the underlying mechanisms. In addition, considering that human tissues are frequently unavailable, using human cells in this in vitro model can avoid the impact of species differences on the results.

We used immortalized NHCs and HCECs for NC permeability testing. The relative accumulated amount of permeated NCs at different times is shown in Figure 6(A) (NHCs) and Figure 6(B) (HCECs). We found that the NCs permeated in a time-dependent manner. In addition, the amounts of FPPP and FPPRP transported into the cells were greatly increased compared with FPP and FPPR, but the amounts of transported FPP and FPPR were alike, indicating that the permeation of NCs was dependent on the PEN peptide instead of the RGD peptide. However, in the NHCs, compared with FPP, the amounts of transported FPPR appeared to be higher ( $p < .05$  at 2 h), and this is consistent with the results of a previous cellular uptake study. The permeability coefficients of NCs at 4 h are shown in Figure 6(C) (NHCs) and Figure 6(D) (HCECs). The permeability coefficients of FPPP were 1.5-fold greater than those of FPP, and the permeability coefficients of FPPRP were 1.6- and 1.5-fold greater than those of FPP and FPPR, respectively (Figure 6C). The permeability coefficients of FPPP were 1.5-fold greater than those of FPP, and the permeability coefficients of FPPRP were 1.2-fold greater than those of FPP and FPPR (Figure 6D). However, there was no significant difference in the permeability coefficients between FPPR and FPP. This may be because of the relatively low level of integrin  $\alpha v \beta 3$  expression in NHCs and HCECs, so the RGD had no contribution to the transmembrane penetration ability of the NCs. In addition, compared with the high permeability conferred by PEN, the RGD



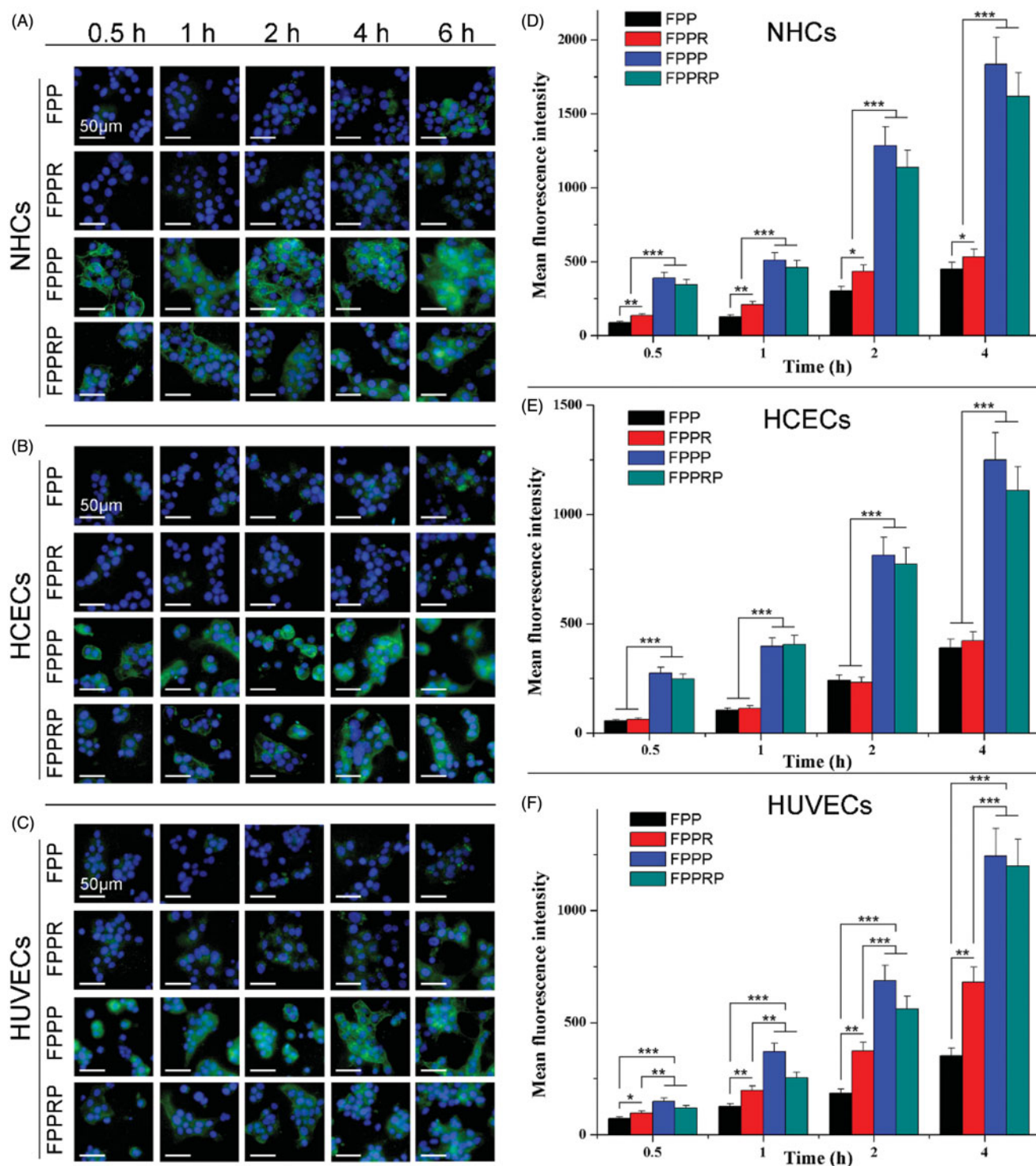


**Figure 5.** Fluorescence microscopy images of the cellular uptake of various NCs at different time in NHCs (A), HCECs (B), and HUVECs (C) (blue for the nuclei, green for the NCs, scale bar = 50  $\mu$ m). Mean fluorescence intensity of various NCs in NHCs (D), HCECs (E), and HUVECs (F) for 4 h ( $n=3$ , mean  $\pm$  SD; \* $p < .05$ , \*\* $p < .01$ , \*\*\* $p < .001$ ).

peptide did not perform well, so we selected the RGD peptide as a targeting ligand rather than a penetrating peptide.

We can conclude that RGD and PEN co-modified NCs can penetrate the conjunctiva and corneal barrier, and substantially increase permeability. What's more, RGD peptide modification did not affect the penetrating effect of the PEN peptide.

### In vivo ocular distribution

To study the intraocular distribution of the NCs after topical instillation, we prepared frozen sections of whole mouse eyes, and then observed the cornea (anterior ocular segment) and retina (posterior ocular segment) using an inverted fluorescence microscope (Figure 7). The frozen

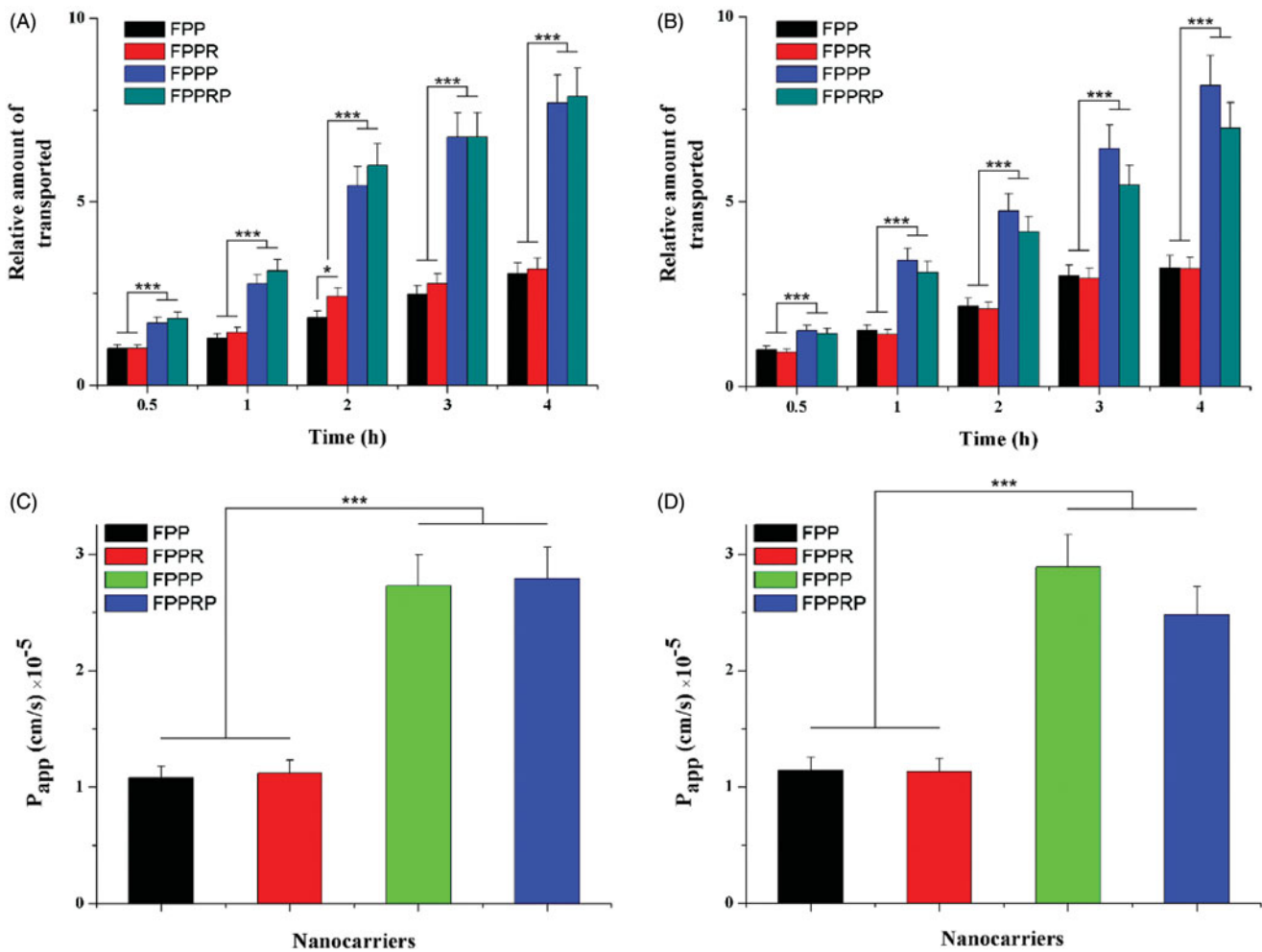


**Figure 6.** In vitro cell model permeation study. Relative numbers of NCs transported across the cell model of NHCs (A) and HCECs (B) for 4 h, permeability coefficients of NCs transported across the cell model of NHCs (C), and HCECs (D) at 4 h ( $n = 3$ , mean  $\pm$  SD; \* $p < .05$ , \*\* $p < .01$ , \*\*\* $p < .001$ ).

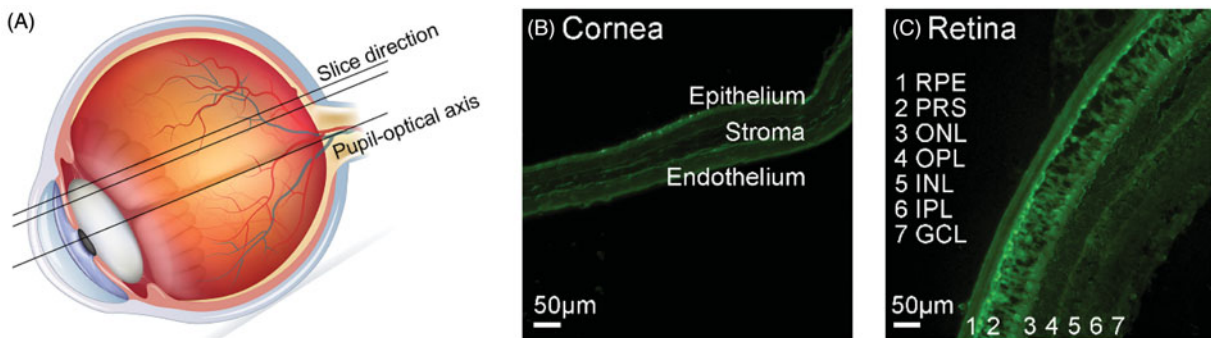


**Figure 7.** Slice direction of the eyeball (A), representative images of the cornea (B) and retina (C) are shown. The general retina structure includes the retinal pigment epithelium (RPE), photoreceptor segments (PRS), outer nuclear layer (ONL), outer plexiform layer (OPL), inner nuclear layer (INL), inner plexiform layers (IPL), and ganglion cell layer (GCL).

sections of the artificial tear fluid group emitted light green fluorescence (Figure 8(E)). After administration, the NCs reached both cornea and retina in 1 h, but the FPP and FPPR groups (Figure 8(A,B)) demonstrated relatively weak green fluorescence, while the FPPP and FPPRP groups (Figure 8(C,D)) demonstrated bright green fluorescence, which was consistent with the results of the in vitro studies. We can conclude that FPPP and FPPRP can penetrate quickly into the cornea and are eliminated after 2 h (Figures 8(C) and

9(D)). FPPP and FPPRP initially penetrated the retinal pigment epithelium of retina within 2 h, and then gradually penetrated the inner side of the retina, and an obvious fluorescence could still be seen at 12 h.

Semi-quantitative analysis was carried out using ImageJ software (Figure 9). Compared with the artificial tear fluid group, an increased fluorescence intensity in the NC groups showed that the NCs can permeate the cornea, and the fluorescence intensity reached a maximum at 2 h and then

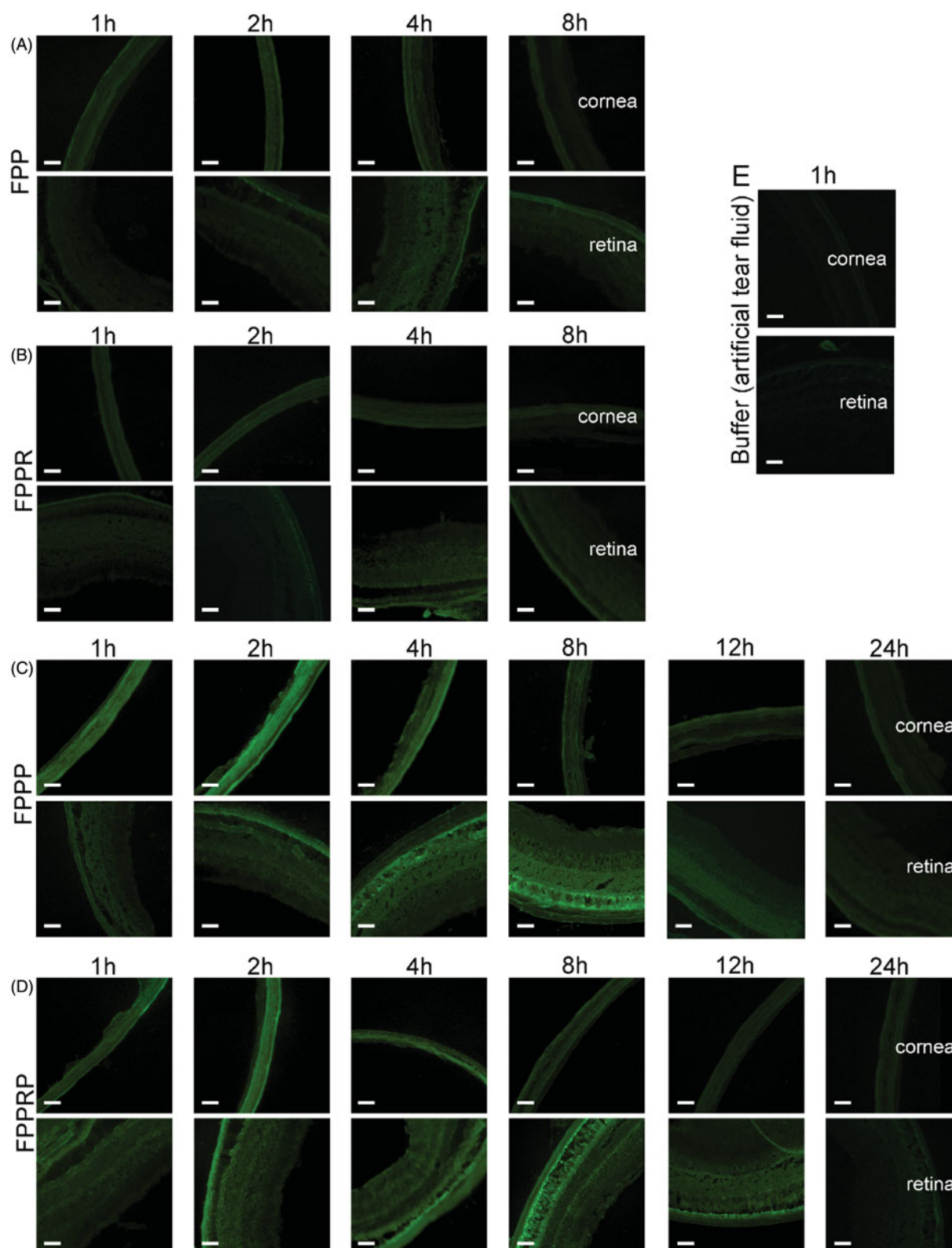


**Figure 8.** Fluorescence images of corneas and retinas of rat bulbus oculi that illustrate distribution and elimination of NCs after topical administration of FPP (A), FPPR (B), FPPP (C), FPPRP (D), or buffer (E). Artificial lacrimal fluid (5  $\mu$ L) to dissolve the NCs (20  $\mu$ M) was instilled into the conjunctival sac of mice every 10 min three times. Scale bar = 50  $\mu$ m.

decayed with time (Figure 9(A)). In addition, compared with the FPP and FPPR groups, the FPPP and FPPRP groups showed stronger fluorescence distribution in the cornea ( $p < .001$ ), which was consistent with the results of the cellular uptake study, indicating that the in vitro cell experiments

predicted the in vivo behavior of the NCs. Compared with the artificial tear fluid group, the fluorescence intensity of the FPP and FPPR groups increased slowly, indicating that the NCs permeated the posterior segments of the eyeball (Figure 9(B)). However, compared with the FPP and FPPR

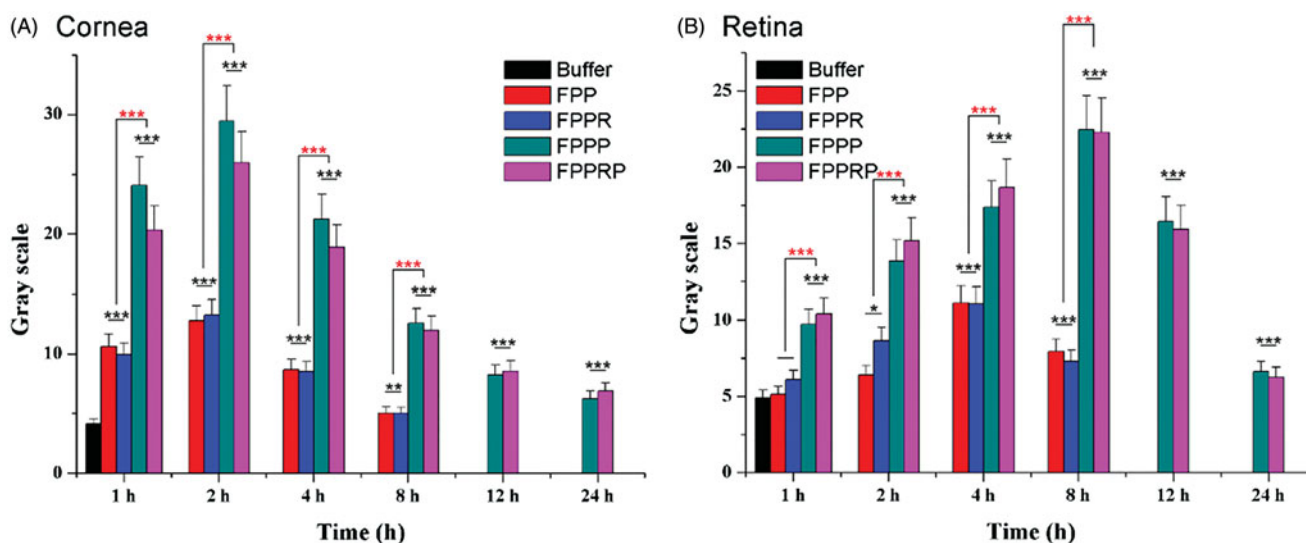


**Figure 9.** Semi-quantitative analysis of mean fluorescent intensity in cornea and retina 1, 2, 4, 8, 12, and 24 h after topical instillation. The retinas and corneas were separated into three regions from top to bottom in the sections, and the mean values of fluorescence intensity were calculated by gray scale. ( $n = 3$ , mean  $\pm$  SD; \* $p < .05$ , \*\* $p < .01$ , \*\*\* $p < .001$ ; “\*” in black, compared with buffer).

groups, the FPPP and FPPRP groups demonstrated higher levels of retinal permeation ( $p < .001$ ), and the fluorescence intensity reached a maximum at 8 h and then decayed with time. In addition, obvious fluorescence could also be seen until 12 h post-application, suggesting that both FPPP and FPPRP resided in the retina persistently.

To investigate the possibility of delivering NPs to the ocular posterior segment through topical administration, intraocular distribution studies were conducted. The NCs (modified with PEN or co-modified with RGD and PEN) have an obvious advantage in delivering therapeutic agents to the ocular posterior segment, and in the current study, they exhibited higher potential in delivering FITC to the ocular posterior segment compared with the FPP and FPPR groups. Nevertheless, FPPP and FPPRP was not statistically different, indicating that the permeation of NCs was dependent on the PEN peptide instead of the RGD peptide and the RGD peptide modification did not affect the penetrating effect of the PEN peptide. In our follow-up studies, the NCs-drug complexes will be constructed and evaluated, the laser-induced CNV rat models will be established for the pharmacodynamic studies, this research can also validate the targeting of NCs to neovascularization at the animal level. In addition, FPPRP will be used in our future investigation, while FPPP as a control. Severe visual loss in AMD is often associated with CNV, and CNV occurs in the blood vessels of the choroid, and then traverses the retinal pigment epithelium layer and continues to grow inside the retina. The relatively high distribution of NCs (carrying drugs through physical entrapment or chemical bonding) in the retina achieved in the current study suggests novel possibilities for the treatment of ocular posterior segment diseases through noninvasive drug administration.

## Conclusions

To overcome the physiological barriers in ocular tissues and barriers to noninvasive delivery of therapeutic agents to the

ocular posterior segment, we successfully established a novel dendrimer-based complex co-modified with RGD and PEN. Cytotoxicity experiments confirmed that the NCs were not significantly cytotoxic at 6 h, and PEG conjugation reduced the cytotoxicity of PAMAM significantly at 24 h. Cellular uptake of RGD-modified NCs involved significant affinity for integrin  $\alpha v \beta 3$ , which validated the NC targeting of the neovasculature. The in vitro permeation study and in vivo ocular distribution results indicated that PEN modification significantly improved the penetration of NCs. Compared with unmodified NCs, PEN-modified NCs showed greater distribution in the ocular posterior segment and prolonged retention in the retina for more than 12 h. In conclusion, the NCs developed in the current study demonstrate excellent membrane permeability, an ability to reach the retina, high biocompatibility, and the ability to carry therapeutic agents such as antiangiogenic drugs and nucleic acids. Consequently, they may create new possibilities in treating posterior ocular diseases. The developed system represents a promising noninvasive intraocular delivery system, which allows the delivery of therapeutic agents to the ocular posterior segment through topical administration.

## Disclosure statement

No potential conflict of interest was reported by the authors.

## Funding

This study was supported by the Natural Science Foundation of Shandong (ZR2014HM062) and the National Science and Technology Major Project (2018ZX09301-017-003).

## ORCID

Xiucheng Yang  <http://orcid.org/0000-0002-0038-8928>



## References

- Ambati J, Ambati BK, Yoo SH, et al. (2003). Age-related macular degeneration: etiology, pathogenesis, and therapeutic strategies. *Surv Ophthalmol* 48:257–93.
- Chu Y, Chen N, Yu H, et al. (2017). Topical ocular delivery to laser-induced choroidal neovascularization by dual internalizing RGD and TAT peptide-modified nanoparticles. *Int J Nanomedicine* 12:1353–68.
- Heier JS, Brown DM, Chong V, et al. (2012). Intravitreal aflibercept (VEGF trap-eye) in wet age-related macular degeneration. *Ophthalmology* 119:2537–48.
- Hennig R, Goepferich A. (2015). Nanoparticles for the treatment of ocular neovascularizations. *Eur J Pharm Biopharm* 95:294–306.
- Huang TC, Huang HC, Chang CC, et al. (2007). An apoptosis-related gene network induced by novel compound-cRGD in human breast cancer cells. *FEBS Lett* 581:3517–22.
- Huckaby JT, Lai SK. (2018). PEGylation for enhancing nanoparticle diffusion in mucus. *Adv Drug Deliv Rev* 124:125–39.
- Inokuchi Y, Hironaka K, Fujisawa T, et al. (2010). Physicochemical properties affecting retinal drug/coumarin-6 delivery from nanocarrier systems via eyedrop administration. *Invest Ophthalmol Vis Sci* 51:3162–70.
- Jain RK, Stylianopoulos T. (2010). Delivering nanomedicine to solid tumors. *Nat Rev Clin Oncol* 7:653–64.
- Jevprasesphant R, Penny J, Jalal R, et al. (2003). The influence of surface modification on the cytotoxicity of PAMAM dendrimers. *Int J Pharm* 252:263–6.
- Koren E, Torchilin VP. (2012). Cell-penetrating peptides: breaking through to the other side. *Trends Mol Med* 18:385–93.
- Li J, Cheng T, Tian Q, et al. (2019). A more efficient ocular delivery system of triamcinolone acetonide as eye drop to the posterior segment of the eye. *Drug Deliv* 26:188–98.
- Li J, Zhang X, Wang M, et al. (2016). Synthesis of a bi-functional dendrimer-based nanovehicle co-modified with RGDyC and TAT peptides for neovascular targeting and penetration. *Int J Pharm* 501:112–23.
- Liu C, Jiang K, Tai L, et al. (2016). Facile noninvasive retinal gene delivery enabled by penetratin. *ACS Appl Mater Interfaces* 8:19256–67.
- Liu C, Tai L, Zhang W, et al. (2014). Penetratin, a potentially powerful absorption enhancer for noninvasive intraocular drug delivery. *Mol Pharmaceutics* 11:1218–27.
- Luo D, Haverstick K, Belcheva N, et al. (2002). Poly(ethylene glycol)-conjugated PAMAM dendrimer for biocompatible, high-efficiency DNA delivery. *Macromolecules* 35:3456–62.
- Luo L, Zhang X, Hirano Y, et al. (2013). Targeted intraceptor nanoparticle therapy reduces angiogenesis and fibrosis in primate and murine macular degeneration. *ACS Nano* 7:3264–75.
- Madaan K, Lather V, Pandita D. (2016). Evaluation of polyamidoamine dendrimers as potential carriers for quercetin, a versatile flavonoid. *Drug Deliv* 23:254–62.
- Malik N, Wiwattanapatapee R, Klopsch R, et al. (2000). Dendrimers: relationship between structure and biocompatibility in vitro, and preliminary studies on the biodistribution of 125I-labelled polyamidoamine dendrimers in vivo. *J Control Release* 65:133–48.
- Mignani S, Rodrigues J, Tomas H, et al. (2018). Bench-to bedside translation of dendrimers: reality or utopia? A concise analysis. *Adv Drug Deliv Rev* 136–137:73–81.
- Millard M, Odde S, Neamati N. (2011). Integrin targeted therapeutics. *Theranostics* 1:154–88.
- Mishra V, Gupta U, Jain NK. (2009). Surface-engineered dendrimers: a solution for toxicity issues. *J Biomater Sci Polym Ed* 20:141–66.
- Nayak K, Misra M. (2018). A review on recent drug delivery systems for posterior segment of eye. *Biomed Pharmacother* 107:1564–82.
- Patel LN, Zaro JL, Shen WC. (2007). Cell penetrating peptides: intracellular pathways and pharmaceutical perspectives. *Pharm Res* 24:1977–92.
- Pennington KL, DeAngelis MM. (2016). Epidemiology of age-related macular degeneration (AMD): associations with cardiovascular disease phenotypes and lipid factors. *Eye Vis (Lond)* 3:34.
- Peynshaert K, Devoldere J, De Smedt SC, et al. (2018). In vitro and ex vivo models to study drug delivery barriers in the posterior segment of the eye. *Adv Drug Deliv Rev* 126:44–57.
- Rofagha S, Bhisitkul RB, Boyer DS, et al. (2013). Seven-year outcomes in ranibizumab-treated patients in ANCHOR, MARINA, and HORIZON: a multicenter cohort study (SEVEN-UP). *Ophthalmology* 120:2292–9.
- Suda K, Murakami T, Gotoh N, et al. (2017). High-density lipoprotein mutant eye drops for the treatment of posterior eye diseases. *J Control Release* 266:301–9.
- Thakur SS, Barnett NL, Donaldson MJ, et al. (2014). Intravitreal drug delivery in retinal disease: are we out of our depth? *Expert Opin Drug Deliv* 11:1575–90.
- Thanh VM, Nguyen TH, Tran TV, et al. (2018). Low systemic toxicity nanocarriers fabricated from heparin-mPEG and PAMAM dendrimers for controlled drug release. *Mater Sci Eng C Mater Biol Appl* 82:291–8.
- Toropainen E, Ranta VP, Talvitie A, et al. (2001). Culture model of human corneal epithelium for prediction of ocular drug absorption. *Invest Ophthalmol Vis Sci* 42:2942–8.
- Votruba M, Gregor Z. (2001). Neovascular age-related macular degeneration: present and future treatment options. *Eye (Lond)* 15:424–9.
- Wang F, Wang Y, Zhang X, et al. (2014). Recent progress of cell-penetrating peptides as new carriers for intracellular cargo delivery. *J Control Release* 174:126–36.
- Wong WL, Su X, Li X, et al. (2014). Global prevalence of age-related macular degeneration and disease burden projection for 2020 and 2040: a systematic review and meta-analysis. *Lancet Glob Health* 2:e106–16.
- Xu Q, Ensign LM, Boylan NJ, et al. (2015). Impact of surface polyethylene glycol (PEG) density on biodegradable nanoparticle transport in mucus ex vivo and distribution in vivo. *ACS Nano* 9:9217–27.
- Xu Q, Kambhampati SP, Kannan RM. (2013). Nanotechnology approaches for ocular drug delivery. *Middle East Afr J Ophthalmol* 20:26–37.
- Yao C, Wang W, Zhou X, et al. (2011). Effects of poly(amidoamine) dendrimers on ocular absorption of puerarin using microdialysis. *J Ocul Pharmacol Ther* 27:565–9.
- Yoncheva K, Lizarraga E, Irache JM. (2005). Pegylated nanoparticles based on poly(methyl vinyl ether-co-maleic anhydride): preparation and evaluation of their bioadhesive properties. *Eur J Pharm Sci* 24:411–9.
- Zhang D, Wang J, Xu D. (2016). Cell-penetrating peptides as noninvasive transmembrane vectors for the development of novel multifunctional drug-delivery systems. *J Control Release* 229:130–9.
- Zhang X, Li X, Hua H, et al. (2017). Cyclic hexapeptide-conjugated nanoparticles enhance curcumin delivery to glioma tumor cells and tissue. *Int J Nanomedicine* 12:5717–32.
- Zhu S, Qian L, Hong M, et al. (2011). RGD-modified PEG-PAMAM-DOX conjugate: in vitro and in vivo targeting to both tumor neovascular endothelial cells and tumor cells. *Adv Mater* 23:H84–89.